Isobaric Yield Distributions in the Interaction of 1.8-GeV Protons with Zr^{96}, Mo^{96}, and Ru^{96}†

NORBERT T. PORILE AND LARRY B. CHURCH*
Chemistry Department, Brookhaven National Laboratory, Upton, New York

(Received 28 August 1963)

Cross sections for the formation of 4 isobars with $A=72$ in the interaction of 1.8-GeV protons with Zr^{96}, Mo^{96}, and Ru^{96}, have been measured. Results have also been obtained for a number of other nuclides with $A=66$–74. It is found that the charge of the most probable product with $A=72$ increases by 0.6 units in going from Zr^{96} to Ru^{96}, resulting in large differences in isobaric yield ratios for the different targets. These results are in qualitative agreement with cascade-evaporation calculations. A strong correlation between the peak position in the isobaric yield curve and the target N/Z value is indicated both by the present results and previous measurements by Kaufman for a number of heavier targets.

I. INTRODUCTION

THE measurement of cross sections for the formation of isobars in high-energy nuclear reactions has received considerable attention in recent years. The investigation of isobaric yield distributions often gives clues about the nature of the nuclear process involved in the reaction and also permits estimation of the cross sections of unmeasured nuclides. Previous investigations[1–4] indicate that the shape of isobaric yield curves is generally not far from Gaussian, with a full width at half maximum of several charge units. Evidence for a double-peaked isobaric yield distribution has been reported recently for the fission of uranium by GeV protons.[5] The most probable charge of the isobaric products has been found[1–5] to range from values corresponding to the near neutron deficient side of stability to those corresponding to the near neutron excessive side.

Miller and Hudis[6] have drawn attention to the fact that a number of isobaric yield ratios for spallation reactions are nearly independent of target and bombarding energy. Moreover, these ratios tend to be similar to those obtained in low-energy compound-nuclear reactions. These observations suggest that, as in low-energy evaporation processes, the properties of the product nuclei play an important role in determining their respective yields. These properties include the energy-level density and its dependence on even-odd and shell effects, the relative values of neutron and proton binding energies, and the height of the Coulomb barrier. Miller and Hudis[6] also conclude that the identity of the target plays a minor role in determining the final isobaric yield ratios provided that the evaporation chain is not too short and starts from nuclei that are not too far from stability. These conclusions, if confirmed by further studies, have important implications for high-energy nuclear reactions. It would appear, for instance, that it might be very difficult to draw conclusions regarding the nature of the progenitors of the product nuclides from the final isobaric yield distribution. On the the other hand, these conclusions suggest certain technical advantages such as ease of interpolation of isobaric yield ratios between different targets.

The above conclusions were based on the rather fragmentary evidence available at the time,[6] and more detailed studies are clearly desirable. Kaufman[4] has recently investigated the isobaric yield distribution in the region of $A=66$–74 for the reactions of indium, gold, and uranium with 2.9-GeV protons. He has found that the isobaric yield ratios have a strong dependence on the target mass, with the production of the more neutron-excessive nuclides being favored from the heavier elements. These results do not, however, constitute a fair test of Miller's hypothesis. As Kaufman points out[4] the reaction mechanism involved in the formation of these products changes from spallation for indium to high-excitation energy fission for gold, and high and low-excitation energy fission for uranium. A more valid test of the above hypothesis, on the other hand, presupposes that the spallation process is involved in all cases.

The present study is an attempt to provide a more definitive answer to the question of whether the evaporation process retains a memory of the original target composition or whether it removes any initial differences, thereby leading to an invariant isobaric yield distribution. In order to make this test as sensitive as possible it seemed clear that the targets should differ in N/Z values as much as possible. On the other hand, the mass difference between target and products should be about equal in all cases in order to minimize any compensating effects that might be introduced by differences in the average lengths of the evaporation chains. It also seemed worthwhile to measure isobaric yield ratios for products variously removed from the stability line in order to observe any systematic trends. Finally, it appeared desirable to investigate cases where the mass difference be-

† Research performed under the auspices of the U. S. Atomic Energy Commission.

* Present address: Department of Chemistry, Carnegie Institute of Technology, Pittsburgh, Pennsylvania.

[1] R. L. Folger, P. C. Stevenson, and G. T. Seaborg, Phys. Rev. **98**, 107 (1955).
[2] A. K. Lavrukhina and L. D. Krasavina, J. Nucl. Energy **5**, 236 (1957.)
[3] J. H. Davies and L. Yaffe, Can. J. Phys. **41**, 762 (1963).
[4] S. Kaufman, Phys. Rev. **129**, 1866 (1963).
[5] G. Friedlander, L. Friedman, B. Gordon, and L. Yaffe, Phys. Rev. **129**, 1809 (1963).
[6] J. M. Miller and J. Hudis, Ann. Rev. Nucl. Sci. **9**, 159 (1959).

tween target and products was larger than 20 mass units in order to ensure reasonably long evaporation chains. Accordingly, we have bombarded targets of Zr^{96}, Mo^{96}, and Ru^{96} with 1.8-GeV protons and measured the cross sections of the $A=72$ isobars, i.e., Zn^{72}, Ga^{72}, As^{72}, and Se^{72}. Results will also be presented for a number of additional gallium and arsenic nuclides. Isobaric yield distribution curves are derived from the measured cross sections and are compared with the results of cascade-evaporation calculations as well as with the results of Kaufman[4] for heavier targets.

II. EXPERIMENTAL

The irradiations were performed in the circulating beam of the Cosmotron at an energy of 1.8 GeV. The target assembly was in a stationary position throughout the run and was protected from low-energy spillout protons by a retractable aluminum shutter. The number of protons striking the target was determined from the Na^{24} disintegration rate in an aluminum foil that was included for this purpose in the target stack. The cross section for the $Al^{27}(p,3pn)$ reaction was taken as 9.6 mb at 1.8 GeV.[7] Targets were usually irradiated for 1-h periods and 11 separate bombardments were performed in the course of this study.

The targets consisted of isotopically enriched materials.[8] The isotopic abundances and chemical composition of the targets are summarized in Table I. The targets were prepared from the enriched isotopes by a previously described[9] sedimentation technique. The procedure consisted briefly of grinding the material to a fine consistency, slurrying it with water or acetone, filtering it onto a carefully leveled disc of filter paper, and covering it with a thin layer of Duco cement. The targets had a thickness of 4–6 mg/cm^2 and had good adherence. The uniformity of the targets was checked visually and targets that appeared to be nonuniform were discarded. In some instances the uniformity was checked by x-ray fluorescence measurements, as described elsewhere.[9] The nonuniformity of most targets was usually less than 15%.

TABLE I. Isotopic abundance and composition of enriched and natural targets.

Target	ZrO_2		MoO_3		Ru	
	Enriched	Natural	Enriched	Natural	Enriched	Natural
Mass No.	(%)	(%)	(%)	(%)	(%)	(%)
90	10.2	51.5				
91	2.0	11.2				
92	3.2	17.1	0.5	15.9		
93						
94	4.6	17.4	0.6	9.0		
95			3.2	15.7		
96	80.0	2.8	89.2	16.5	94.9	5.5
97			3.3	9.5		
98			2.7	23.8	0.4	1.9
99					1.3	12.7
100			0.5	9.6	0.8	12.6
101					0.8	17.1
102					1.2	31.6
103						
104					0.6	18.6

In addition to the targets prepared from the enriched materials, targets of natural zirconium, molybdenum, and ruthenium were also irradiated. These experiments were performed since it was necessary to correct the results for the contribution from minor isotopic constituents of the enriched targets. The contribution to the observed activities from impurities in the backing material was not determined. Previous studies[9] have shown, however, that this effect is completely negligible for products in the mass region of interest.

The target stack consisted of the target foil and of three 0.001-in. thick aluminum foils on the upstream side of the target. The central foil was used to monitor the beam intensity. The other aluminum foils were used to compensate for recoil loss and to protect the monitor foil from recoils originating in the target foil. The latter was oriented so that forward recoils were stopped in the filter paper backing and backward recoils in the Duco layer. After irradiation the leading edge of the target stack was carefully trimmed off and the foils were cut from the target holder.

The chemical separation procedures were the same as those used by Kaufman and the details are given in his papers.[4,10] Minor modifications were necessary because the targets were dissolved in different media. ZrO_2 was thus dissolved in HNO_3+HF, MoO_3 in NH_4OH, and Ru in 6 M NaOH solution saturated with Cl_2. Carriers of the elements to be separated were in all cases present in the dissolving solutions. The arsenic and gallium samples were separated directly for radioactivity assay. The disintegration rates of Se^{72} and Zn^{72}, on the other hand, were determined from measurements on their decay products, As^{72} and Ga^{72}, respectively. The selenium and zinc samples were consequently allowed to stand after purification to permit equilibration, and arsenic and gallium were then separated.

The radioactivity measurements were performed in the manner described by Kaufman,[10] who lists the pertinent decay scheme information for the nuclides of interest. Briefly, the disintegration rates of Ga^{66}, Ga^{67}, Ga^{72}, Ga^{73}, As^{71}, As^{72}, and As^{74} were determined by γ-ray pulse spectrometry with a 3-in.×3-in. NaI(Tl) detector connected to a 100-channel pulse-height analyzer. The disintegration rates of Se^{72} and Zn^{72}, as determined by measurements on As^{72} and Ga^{72}, were too low for this type of assay and beta-proportional counters with backgrounds of either 8–10 or 0.2 cpm were employed. The beta-detection results were corrected for the variation of counting efficiency with sample thickness by means of empirically determined[11] correction factors.

[7] J. B. Cumming, J. Hudis, A. M. Poskanzer, and S. Kaufman, Phys. Rev. **128**, 2392 (1962).
[8] Obtained from Oak Ridge National Laboratory.
[9] N. T. Porile and S. Tanaka, Phys. Rev. **130**, 1541 (1963).
[10] S. Kaufman, Phys. Rev. **126**, 1189 (1962).
[11] S. Kaufman (private communication).

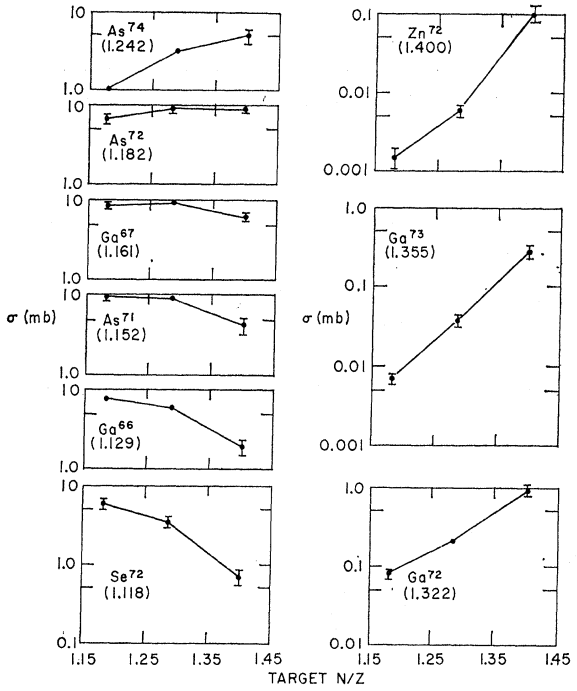

FIG. 1. Dependence of the independent formation cross sections on target N/Z. The targets are Ru^{96}, Mo^{96}, and Zr^{96}. The numbers in parentheses are the product N/Z values.

III. RESULTS

The measured cross sections are summarized in Table II. The listed values have been corrected for the contribution from minor isotopic constituents of the targets. These corrections were usually less than 15% except for the most neutron deficient products from Zr^{96}. The cross section for Se^{72} from this target thus had to be reduced by a factor of 2. The correction was made on the assumption that the relative abundance of the extraneous isotopes was the same in the enriched and normal materials. The data in Table I indicate that this assumption is valid. We estimate an error of about 15% in this particular correction. The results are the average of either 2 or 3 separate determinations and the errors include both the standard deviation of the mean and an estimate of systematic errors. The products have been labeled in Table II to indicate whether their yields are independent or cumulative. The cross section for Ga^{66} includes a small fraction of the yield of Ge^{66}. The numbers in parenthesis refer to the estimated independent cross sections in those cases where they differ from the measured cumulative values. They were obtained on the basis of isobaric yield distribution curves discussed in the following section. We shall refer only to these independent cross sections in the subsequent discussion.

TABLE II. Experimental cross sections at 1.8 GeV.

Product	Target Zr^{96} (mb)	Target Mo^{96} (mb)	Target Ru^{96} (mb)
Zn^{72a}	0.11±0.02(0.10)	0.006±0.001	0.0016±0.0004
Ga^{66b}	2.0±0.4	6.0±0.2	7.8±0.3
Ga^{67a}	6.4±0.8(6.3)	10.5±0.7(9.6)	11.3±0.7(9.0)
Ga^{72b}	0.9±0.1	0.22±0.02	0.08±0.01
Ga^{73a}	0.34±0.05(0.30)	0.040±0.007(0.039)	0.008±0.001(0.007)
As^{71a}	4.4±1.0(4.3)	9.7±0.4(9.4)	11.2±1.0(9.7)
As^{72b}	9.0±1.0	9.5±1.0	7.0±1.0
As^{74b}	5.1±1.0	3.3±0.2	1.1±0.2
Se^{72a}	0.70±0.15	3.6±0.5(3.5)	6.5±1.0(6.0)

[a] Cumulative yield; [b] independent yield. The numbers in parentheses are estimates of the independent yields.

The cross sections for the independent formation of the various products are plotted in Fig. 1 as a function of target N/Z. It is seen that the shapes of the curves change in a striking manner with the N/Z value of the product. The cross sections for the formation of the most neutron excessive nuclides, Zn^{72} and Ga^{73}, are larger by nearly 2 orders of magnitude for Zr^{96} than for Ru^{96}. As the products become increasingly neutron deficient the cross sections from Zr^{96} decrease relative to those from Ru^{96}, and the yields for all 3 targets become approximately equal for product N/Z values of 1.16–1.18. As the products become even more neutron deficient, the slope of the curves reverses and the largest cross sections are obtained for the Ru^{96} target.

The above trends are also strikingly revealed in Figs. 2 and 3, which show the variation of $\sigma_{Mo^{96}}/\sigma_{Zr^{96}}$, $\sigma_{Ru^{96}}/\sigma_{Mo^{96}}$, and $\sigma_{Ru^{96}}/\sigma_{Zr^{96}}$ with product N/Z. It is seen that both $\sigma_{Ru^{96}}/\sigma_{Mo^{96}}$ and $\sigma_{Mo^{96}}/\sigma_{Zr^{96}}$ decrease nearly monotonically with increasing product N/Z. The Ru/Mo cross-section ratios appear to have a smaller N/Z dependence than the Mo/Zr ratios, particularly for large

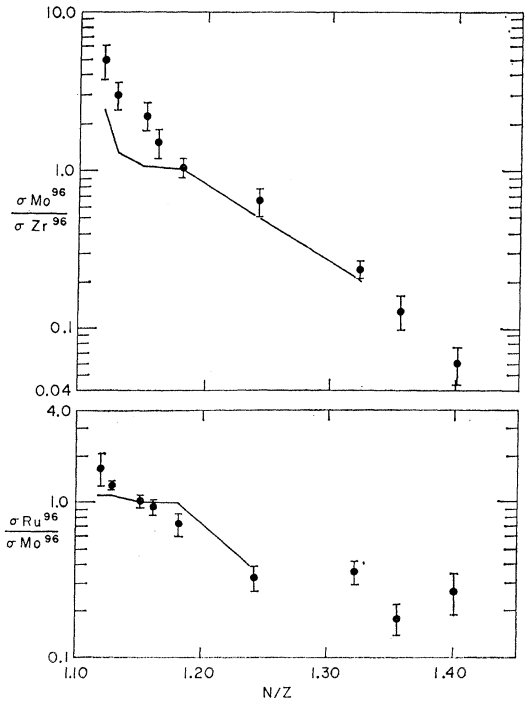

FIG. 2. Variation of cross section ratios with the product N/Z. The solid lines are the result of cascade-evaporation calculations.

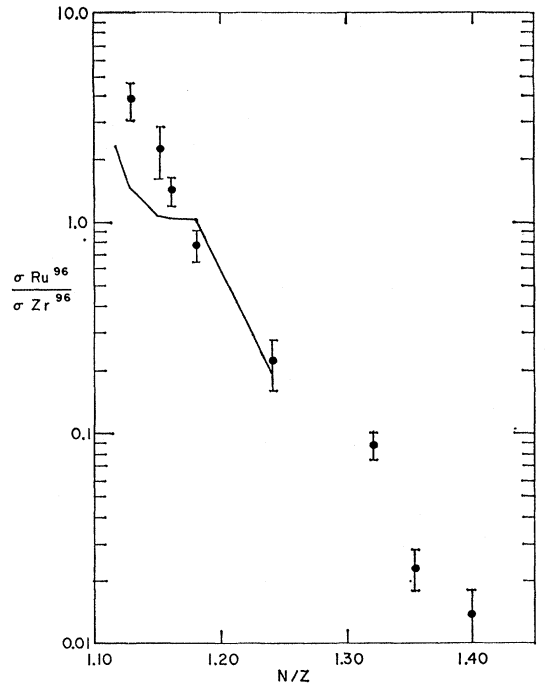

FIG. 3. Variation of the Ru^{96}/Zr^{96} cross-section ratio with product N/Z. The solid line is the result of cascade-evaporation calculations.

N/Z values. The Ru/Zr ratio curve, which is the product of the other two curves, predictably exhibits a very sharp N/Z dependence. The value of $\sigma_{Ru^{96}}/\sigma_{Zr^{96}}$ thus varies from 8.6 for Se^{72} to 0.014 for Zn^{72}. In spite of the large relative yields of neutron excessive products from Zr^{96} it can be seen that the absolute cross sections of these products are small for all the targets under consideration. This is in accord with the known tendency of the spallation process to favor the formation of neutron deficient products.

IV. DISCUSSION

A. Isobaric Yield Distributions

The measured cross sections may be used to construct isobaric yield distribution curves on the assumption that the total isobaric yield is approximately constant for $A=66$–74. The resulting curves, plotted against the N/Z of the products, are shown in Figs. 4–6. The independent yields of products for which only cumulative yields were available were established by successive approximation. The principle used in this procedure was to require the interpolated independent yields for a particular isobaric chain to add up to the measured cumulative yield for that chain. It is seen that all 3 curves exhibit a single peak that moves to larger N/Z value with increasing target N/Z. The shift in the charge of the most probable product at $A=72$, in going from Ru^{96} to Zr^{96}, is $\Delta Z_p=0.6$. The curves are not symmetric about the peak but decrease more sharply on the low

TABLE III. Isobaric cross section at $A=72$.

Target	σ_{exp} (mb)	σ_{calc} (mb)
Zr^{96}	14.8±1.3	25.3±1.6
Mo^{96}	16.1±1.2	26.3±1.7
Ru^{96}	14.7±1.4	24.1±1.5

N/Z side. The full width at half-maximum is approximately the same for all the targets.

The isobaric yield curves may be used to estimate the yield of stable Ge^{72}, thereby permitting a determination of the total cross section for $A=72$. The results are summarized in Table III. It is seen that, within the limits of error, the cross sections for all 3 targets are equal to about 15 mb. It may be concluded that although the individual isobaric yields differ widely, the total yield at $A=72$ is independent of target composition.

Kaufman[4] has previously determined the isobaric yield distribution in the mass region of interest for a number of targets. Although his experiments were performed at 2.9 GeV, a comparison with the present results should be useful in pointing out any systematic trends. The variation of the N/Z value of the most probable product with the N/Z of the target is shown in Fig. 7. for both the $A=96$ targets as well as for In, Au, and U. It is seen that the most probable N/Z value increases nearly linearly with target N/Z although there appears to be a somewhat sharper increase in going to U. This is probably indicative of the effect of low deposition energy fission of U. It is interesting to note, however, that the position of the maximum in the isobaric yield curve correlates very

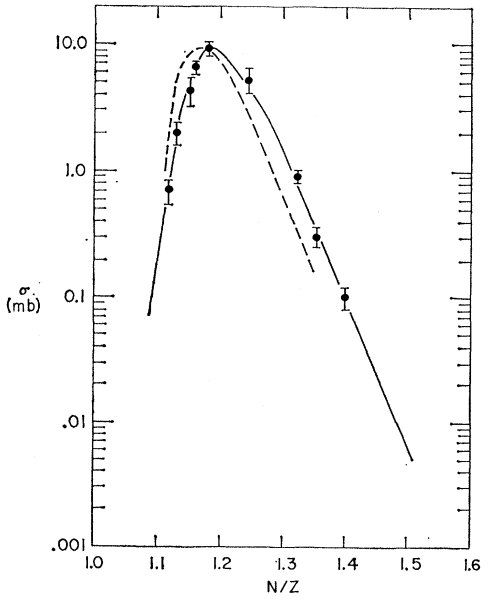

FIG. 4. Isobaric yield distribution curve for Zr^{96}. The solid curve connects the points for the independent-formation cross sections. The dashed line is the normalized result of a cascade-evaporation calculation.

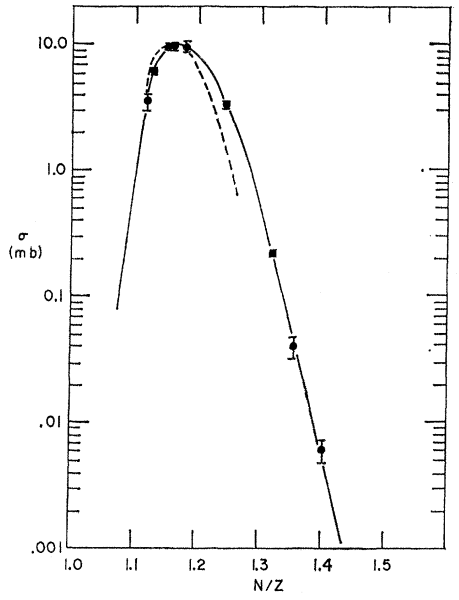

FIG. 5. Isobaric yield distribution curve for Mo^{96}. See Fig. 4 for details.

well with the target N/Z, in spite of the wide range in target A and the previously mentioned differences in mechanism.

The results of the present study may be compared with cascade-evaporation calculations. The results for the cascade process were obtained from the Monte Carlo calculation of Metropolis *et al.*[12] for 1.8-GeV protons incident on Ru^{100}. The residual nuclei resulting from the knock-on cascade were first shifted in Z and A to correspond to the targets in question. In the case of Ru^{96} and Zr^{96} small additional adjustments in the distribution of cascade products were made to account for the difference in N/Z values between these targets and Ru^{100}. The calculations of Metropolis *et al.*[12] indicate that neutrons and protons are emitted in the course of the cascade in a ratio that, on the average, is approximately given by the target N/Z. The shifted products for Ru^{96} and Zr^{96} were accordingly corrected by respectively converting every 48th emitted neutron into a proton and vice versa.

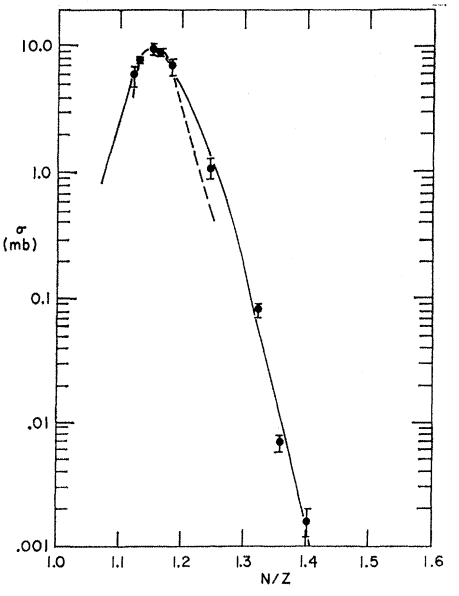

FIG. 6. Isobaric yield distribution curve for Ru^{96}. See Fig. 4 for details.

The corrected distributions of residual nuclei were used as the starting point for a Monte Carlo evaporation calculation based on the treatment due to Dostrovsky *et al.*[13] The calculations were performed on an IBM 7094 computer using a nuclear radius parameter $r_0 = 1.5$ F and a level density parameter $a = A/10$. In order to improve the statistics of the calculation, 25 evaporations were performed for each of approximately 400 starting nuclei.

The calculated isobaric yield curves are shown in Fig. 8. The curves are based on the formation cross sections for all nuclei in the $A = 66$–74 mass region. The individual points scatter about the curves with a standard deviation of approximately 10%. It is seen that the curves exhibit the same qualitative trends as the experimental distributions, i.e., the most probable value of N/Z increases with the target N/Z and the drop off in cross section is steeper on the neutron deficient side of the peak.

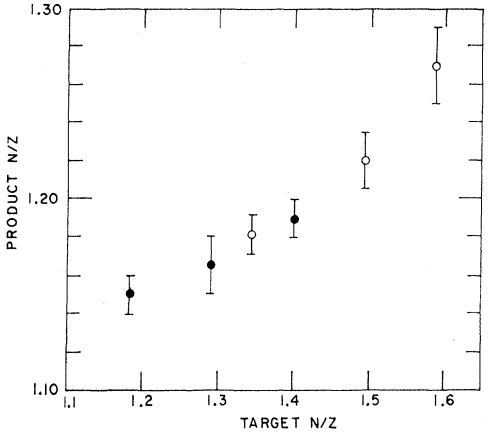

FIG. 7. Variation of N/Z value of most probable product with target N/Z. ●—results of this study; ○—results of Kaufman for In, Au, and U targets.

The calculated curves are compared with the experimental ones in Figs. 4–6. For the purposes of this comparison the calculated curves are based exclusively on the independent cross sections of the measured nuclei. The calculated curves have been normalized at the peak in order to facilitate comparison of the curve shapes. It is seen that the calculation predicts a sharper drop off on

[12] N. Metropolis, R. Bivins, M. Storm, J. M. Miller, G. Friedlander, and A. Turkevich, Phys. Rev. **110**, 204 (1958).

[13] I. Dostrovsky, Z. Fraenkel, and G. Friedlander, Phys. Rev. **116**, 683 (1959).

the neutron-excessive side of the peak for all 3 targets. Unfortunately the statistics of the calculation are not good enough to give information on the most neutron-excessive products. The positions of the maxima as well as the relative yields on the neutron-deficient side of them are well reproduced by the calculation for Ru^{96} and Mo^{96}. The calculated curve for Zr^{96}, however, appears to be uniformly shifted to lower N/Z values. The calculated ratios of cross sections for the different targets are compared with the experimental ratios in Figs. 2–3. Once again it is seen that the trend of the calculated ratios is similar to that of the measured values although factor-of-2 discrepancies may be noted.

The calculated isobaric cross sections at $A=72$ are compared with the experimental values in Table III. It is seen that the calculated values are about 70% larger than the experimental ones. This discrepancy is undoubtedly connected with the failure of the calculation to account for the cross sections of simple nuclear reactions,[14,15] where discrepancies of up to a factor of 9 have been noted. Also, the calculation does not take into account the occurrence of fission which accounts for nearly 10% of the reaction cross section at 2 GeV.[16] Since the calculated total reaction cross section[12] is in agreement with experimental values, it follows that an underestimate of cross sections in one region of yields must be balanced by an overestimate in another region.

B. Isobaric Yields and Their Ratios

The previous discussion has already indicated that the hypothesis of invariant isobaric yield ratios does not hold for the cases under consideration. In this part of the discussion we consider these ratios explicitly and attempt to understand the observed behavior.

The isobaric yield ratios for $A=72$ are summarized in Table IV. It is seen that the ratios vary in a systematic way with the N/Z of the target. Moreover, the magnitude of this variation is approximately independent of whether the products are neutron excessive or neutron deficient. Some of the isobaric ratios of interest have been measured in low-energy alpha induced reactions and the results are given in Table IV. These ratios are seen to fall in line with the values for the more neutron

TABLE IV. Summary of isobaric yield ratios.

Target	$\sigma_{As^{72}}/\sigma_{Se^{72}}$	$\sigma_{Ga^{72}}/\sigma_{As^{72}}$	$\sigma_{Zn^{72}}/\sigma_{Ga^{72}}$
Zr^{96}	12.8±3.1	0.10±0.016	0.11±0.03
Mo^{96}	2.7±0.5	0.023±0.003	0.027±0.005
Ru^{96}	1.17±0.26	0.011±0.002	0.020±0.006
Zn^{70a}			0.014
Ge^{70b}	1.7		

[a] From S. Amiel, Phys. Rev. 116, 415 (1959). The quoted ratio is for the highest excitation energy; ratio is lower at lower excitation energies.
[b] Data from same reference as a. The average ratio over most of the excitation energy range is given.

[14] N. T. Porile, Phys. Rev. 125, 1379 (1962).
[15] N. T. Porile and S. Tanaka, Phys. Rev. 132, 397 (1963).
[16] E. W. Baker and S. Katcoff, Phys. Rev. 126, 729 (1962).

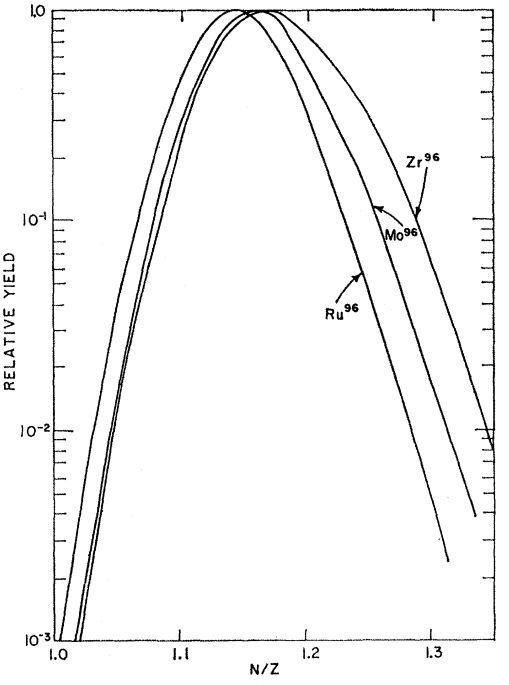

FIG. 8. Isobaric yield distribution curves obtained from cascade-evaporation calculations.

deficient targets. This result is quite reasonable since the compound nuclei have fairly low N/Z values. Another indication of the correlation between isobaric yield ratio and target N/Z is given in Fig. 9, where the present results are compared with Kaufman's data.[4]

The difference between the present results and those quoted by Miller and Hudis[6] may be understood with

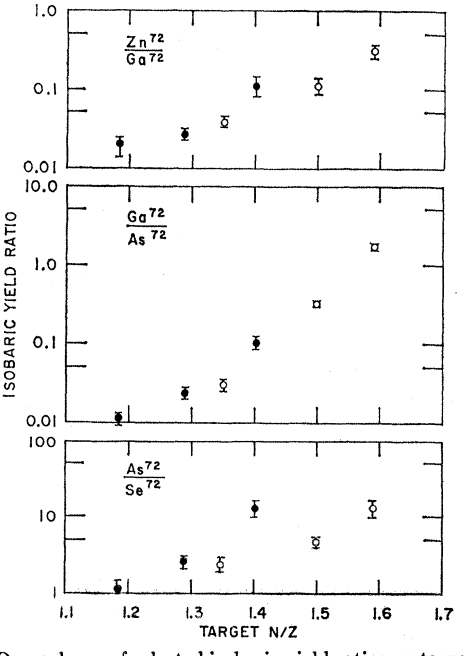

FIG. 9. Dependence of selected isobaric yield ratios on target N/Z. ●—this work; ○—Kaufman's data for In, Au, and U.

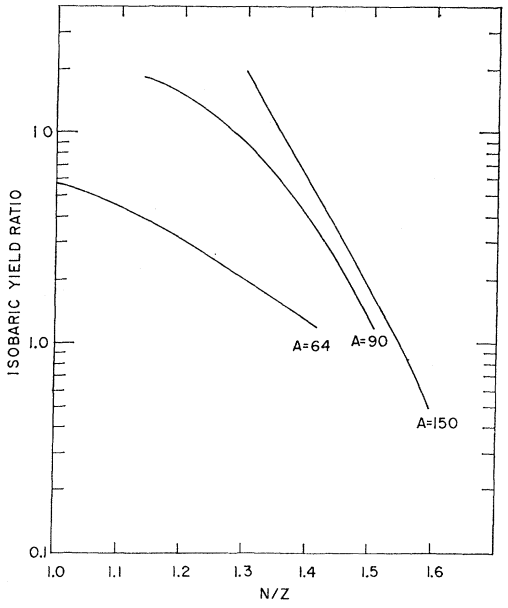

FIG. 10. Dependence of some calculated isobaric yield ratios on the N/Z of the starting nucleus. The calculation is for evaporation from a given starting nuclide. The curves are labeled with the A of the starting nucleus and refer, in order of increasing target A, to $\sigma_{V^{48}}/\sigma_{Ti^{48}}$, $\sigma_{As^{72}}/\sigma_{Ge^{72}}$, and $\sigma_{Ce^{132}}/\sigma_{La^{132}}$.

the aid of the following calculation. We have computed isobaric yield ratios for products with $A=48$, 72, and 138 formed by evaporation from a number of single nuclides with $A=64$, 90, and 150, respectively. The resulting ratios for adjacent isobars are plotted against the N/Z of the starting nuclide in Fig. 10. It is seen that the dependence on N/Z increases with increasing target mass number. The results quoted by Miller and Hudis[6] are for isobars with A ranging from 45 to 55 and for target $A\leq 75$. Moreover their targets in all cases consisted of normal isotopic material, and therefore did not cover a large N/Z range. For instance their quoted results for the Cr^{48}/V^{48} yield ratio, indicate a variation of about a factor of 2 for targets with N/Z ranging from 1.15 to 1.27. It is seen from the curve for $A=64$ in Fig. 10 that such a variation is perfectly reasonable. It may be concluded that the hypothesis advanced by Miller and Hudis[6] holds only for targets with nearly identical N/Z values especially if the products have $A\leq 60$.

The increase with A of the isobaric yield ratio dependence on target N/Z depicted in Fig. 10 is of some importance. We believe that this trend is due to the following two characteristics of the evaporation process. First, the formation during an evaporation chain of nuclides that are far from stability occurs with increasing probability as the target mass increases. This is due to the decrease of the slope of the sides of the stability valley with increasing mass number. For instance, the number of particle-stable isobars estimated by Cameron[17] increases from 10 at $A=41$, to 15 at $A=71$, to 21 at $A=131$. As a consequence, evaporation from a nuclide with either low or high N/Z can more readily preserve this N/Z value in the heavy element region. In the light element region the more rapid decrease in neutron or proton binding energies as one moves away from the stability line tends to channel the evaporation path along a relatively narrow band of nuclides. Second, the distribution in isobaric products prior to the last one or two evaporation steps is more effectively preserved in the terminal step at high mass numbers. This fact is a consequence of the increase in the coulomb barrier against proton emission with increasing A. In the light-mass region proton evaporation competes effectively with neutron evaporation, permitting a further smearing out of the original N/Z distribution during the final deexcitation steps.

We conclude this discussion with a consideration of the dependence of the isobaric cross section at $A=72$ as well as that of several individual cross sections on target N/Z. The data of Kaufman[4] and of this study are plotted in Fig. 11. The isobaric cross section for $A=72$ is seen to be nearly independent of N/Z for targets which can give rise to the products by spallation. The cross section decreases for Au, and then increases for U reflecting the variation of the fission cross section in the heavy element region. The cross sections for the formation of As^{72}, a product with a high yield from all the targets, show approximately the same behavior as the isobaric cross sections. It is quite obvious that the dependence of these cross sections on target N/Z is not particularly revealing and that a plot of σ versus target A would point up the features of interest more clearly. By contrast, however, the dependence of the yields of the more neutron exces-

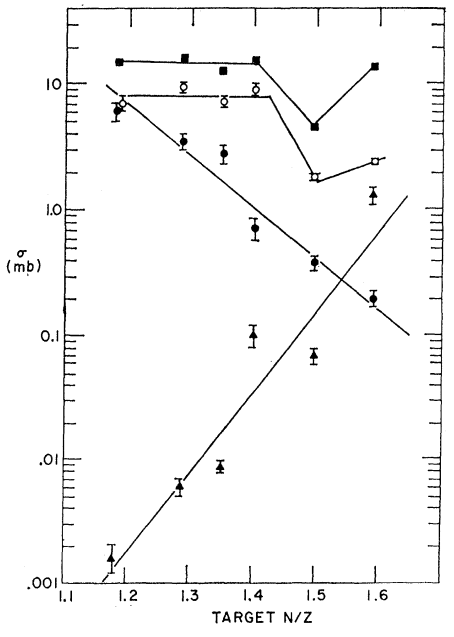

FIG. 11. Dependence of experimental cross sections on target N/Z. ■—total isobaric cross section for $A=72$; ○—As^{72}; ●—Se^{72}; ▲—Zn^{72}. The data are from Kaufman's paper and from the present work.

[17] A. G. W. Cameron, Atomic Energy of Canada Ltd., AECL No. 433 (1957) (unpublished).

sive or deficient products on target N/Z is seen to be strong and markedly different from that of the isobaric cross section. This point illustrates the danger of drawing conclusions about the dependence of isobaric yields on target A or N/Z from measurements on single isobars.

V. CONCLUSIONS

The present investigation of the isobaric yield distribution at $A=66$–74 resulting from spallation of 3 targets with $A=96$ by 1.8 GeV protons reveals the dependence of this distribution on the N/Z value of the target. A change of 4 charge units for the targets thus results in a concomitant change in Z_p at $A=72$ of 0.6 units. This shift in turn results in order of magnitude differences in isobaric yield ratios obtained for the different targets. These conclusions indicate that while the hypothesis of invariant isobaric yield ratios[6] for spallation reactions may hold true in a comparison of targets with similar N/Z values, it is not generally valid. The correlation with N/Z is further confirmed in the comparison of the present results with those of Kaufman[4] and is also in agreement with cascade-evaporation calculations. It is of interest to note that the correlation of the Z_p values, isobaric yield ratios, and cross sections of very neutron deficient or excessive products with target N/Z is only weakly affected by the obvious differences in the reaction mechanism for the various targets studied by Kaufman[4] and by us. It would be of interest to perform measurements of this type in other mass regions in order to test the generality of these notions.

ACKNOWLEDGMENTS

The cooperation of the operating staff of the Cosmotron is appreciated. The chemical yield measurements were ably performed by Dr. R. W. Stoenner, Dr. J. K. Rowley, and members of the analytical chemistry group. Special thanks are due to Dr. S. Kaufman for making the results of his counter efficiency measurements available to the authors. The results of the Monte Carlo cascade calculations were kindly made available by Dr. G. Friedlander. We wish to thank Dr. S. Katcoff for a critical reading of the manuscript.

PHYSICAL REVIEW VOLUME 133, NUMBER 2B 27 JANUARY 1964

Elastic Scattering of Protons by Fe^{56}, Fe^{58}, and Ni^{58} at 10.9 and 11.7 MeV

J. BENVENISTE AND A. C. MITCHELL
Lawrence Radiation Laboratory, University of California, Livermore, California

AND

C. B. FULMER
Oak Ridge National Laboratory, Oak Ridge, Tennessee*

(Received 5 August 1963)

Differential cross sections for elastic scattering of protons from Fe^{56}, Fe^{58}, and Ni^{58} were measured and compared. Differences in positions of the maxima and minima are observed; when compared with the results of extensive optical model analyses of other data these are shown to be consistent with a nuclear symmetry dependence of the real nuclear-potential well depth. A comparison of the $A=58$ data with previously reported $A=64$ data shows the positions of maxima and minima in the differential elastic-scattering cross sections to be much more sensitive to differences of $(N-Z)/A$ than to differences in nuclear deformation.

INTRODUCTION

THEORETICAL studies[1] have shown that there are reasons to expect a dependence of the real nuclear potential well depth V on the nuclear symmetry parameter $(N-Z)/A$;

$$V=V_0\pm[(N-Z)/A]V_1 \quad (1)$$

for protons and neutrons, respectively. In a recent optical model analysis of proton elastic scattering in the range of 9 to 22 MeV[2] the observed increase of the real well depth as a function of mass number was explained in part by a nuclear symmetry term in the potential. Optical model analyses of proton-nucleus elastic-scattering data[3,4] have shown that maxima and minima in elastic-scattering angular distributions occur at angular positions that are determined mainly by VR^n, where R is the nuclear radius and n increases with proton energy. It thus seems that the experimental study of proton-nucleus elastic scattering by isobars should be one of the most direct ways to obtain experimental information about the role of the nuclear symmetry parameter in elastic scattering and hence the effect it has on the real

* Operated for the U. S. Atomic Energy Commission by Union Carbide Corporation.

[1] A. M. Lane, Phys. Rev. Letters **8**, 171 (1962); an extensive bibliography is given in Ref. 5.

[2] F. G. Perey, Phys. Rev. **131**, 745 (1963).

[3] A. E. Glassgold, W. B. Cheston, M. L. Stein, S. B. Schuldt, and G. W. Erickson, Phys. Rev. **106**, 1207 (1957).

[4] A. E. Glassgold and P. J. Kellog, Phys. Rev. **107**, 1372 (1957).